The effect of in-plane mass anisotropy on the properties of high temperature superconductors in states of mixed symmetry

2009 J. Phys.: Condens. Matter 21 405702

(http://iopscience.iop.org/0953-8984/21/40/405702)

J. Phys.: Condens. Matter **21** (2009) 405702 (11pp) doi:10.1088/0953-8984/21/40/405702

The effect of in-plane mass anisotropy on the properties of high temperature superconductors in states of mixed symmetry

Madhuparna Karmakar and Bishwajyoti Dey

Department of Physics, University of Pune, Pune 411007, India

E-mail: madhu@physics.unipune.ernet.in and bdey@physics.unipune.ernet.in

Received 9 March 2009, in final form 10 August 2009
Published 14 September 2009
Online at stacks.iop.org/JPhysCM/21/405702

Abstract

Experiments have suggested that the high-T_c cuprate YBCO shows marked anisotropy in penetration depth and coherence length measurements. In order to take into account the presence of this anisotropy in the system and its corresponding effect on the various properties of the high-T_c superconducting materials, we have developed an anisotropic two-order parameter Ginzburg–Landau (GL) theory involving a mixed symmetry state of the order parameter components. For this we have generalized a two-order parameter GL theory, recently developed for the isotropic high-T_c superconductors involving a mixed symmetry state of the order parameter components (Karmakar and Dey 2008 *J. Phys. Condens. Matter* **20** 255218), in which the effect of the presence of in-plane anisotropy has been taken into account by an effective mass approximation, with the anisotropy being characterized by the parameter $\gamma = m_x/m_y$. The work goes beyond the limitations of the earlier studies in this field as it enables us to carry out a detailed study of the various properties of the system over the entire range of applied magnetic field and wide range of temperature for arbitrary values of the GL parameter κ_y and vortex lattice symmetry. The model successfully explains not only the observed oblique vortex lattice structure in the presence of in-plane anisotropy but also the experimentally observed angle between the primitive axes of the vortex lattice. The generation of two-fold symmetry of the vortices in the presence of in-plane anisotropy, for a very low applied magnetic field can also be analyzed by our model. We have also compared our theoretical results with various other experiments on high-T_c cuprate YBCO.

1. Introduction

A critical issue in the study of the properties of high-T_c superconductors, is the pairing symmetry of the order parameter components. Experimental observations have predicted the possibility of a d-wave pairing symmetry, i.e. the $d_{x^2-y^2}$ pairing state with lines of nodes in the energy gap. The possibility of a d-wave pairing symmetry has been predicted by phase sensitive experiments such as Josephson junction experiments, superconducting quantum interference device (SQUID) measurements etc [2–5]. However, most recent experiments [6–9] show the possibility of a mixed symmetry state of the order parameter components, where the bulk pairing symmetry is d-wave, along with the admixture of a small s-wave component. Sigrist *et al* have shown that a small s-wave component will be present in addition to a dominant d-wave component in YBCO [10]. In fact many of the inconsistencies of the observations of the experiments supporting the presence of a d-wave pairing symmetry could be explained by allowing for a mixed symmetry state of the order parameter components and it is suggested that the mixed symmetry scenario can prove to be the origin of several unusual effects observed experimentally in HTS, namely the unusual upward curvature of the plot of temperature versus the upper critical magnetic field (H_{c2}) [11], the pseudo-gap effects in HTS [12], the nonmagnetic impurity effects in HTS leading

to an energy gap [13] and the superconducting fluctuation effects in HTS [14]. For a detail account of the experimental studies which supports the above mentioned scenarios, see [1]. The mixed symmetry pairing scenario has also been used to explain the origin of fractional vortices in HTS [15, 16] and the influence of the twin boundary in Josephson junction tunneling [17].

The presence of a mixed symmetry state of the order parameter components in high-T_c superconducting materials has been attributed to the very complex structure of these materials, particularly the existence of the CuO chains in the system. The presence of the CuO chains and the resulting orthorhombic distortion of the system gives rise to an in-plane gap anisotropy in the system [18, 19]. Experimental manifestations of this energy gap anisotropy have been many. Whether it is the Raman scattering experiment of $YBa_2Cu_4O_8$ [20] and $YBa_2Cu_3O_7$ [21, 22] or the photo-emission spectra of $YBa_2Cu_3O_{7-\delta}$ [18], all have supported the existence of an energy gap anisotropy in the high-T_c cuprates. Angle resolved electron tunneling measurements have also indicated the presence of an in-plane anisotropy in the energy gap of the order of $\Delta_a/\Delta_b = 1.5$ [6].

Apart from the in-plane anisotropy in the energy gap, there are other properties of the high-T_c superconductors, namely penetration depth, coherence length, vortex lattice structure etc which demonstrate the presence of in-plane anisotropy. Microwave surface impedance measurements have shown the presence of in-plane anisotropy in the penetration depth [23] with the anisotropy parameter γ determined to be equal to $\gamma = 2.4$. The small angle neutron scattering (SANS) [24] and scanning tunneling microscopy (STM) [25] measurements carried out on high-T_c cuprates have indicated the presence of an oblique structure of the flux line lattice suggesting the presence of an anisotropy in the system. The vortex imaging carried out by using STM measurements showed that the angle between the primitive axes is $\beta \approx 77^\circ \pm 5^\circ$, the vortex cores have been found to be elongated, with the ratio of the axes being 1.5. The corresponding ratio of the coherence lengths as determined by the structure of the vortices amounts to 1.5 in agreement to the anisotropy determined by the penetration depth measurements [23].

It must be noted that such an oblique vortex lattice structure can be obtained by taking into consideration only the mixed symmetry state of the order parameter components even in the absence of an explicit in-plane anisotropy [1]. However, such an isotropic model fails to give the correct value of the angle between the primitive axes of the lattice, indicating that the mixed symmetry scenario alone cannot explain the experimentally observed features of the high-T_c cuprates. In the later sections where we discuss in detail the vortex lattice structures and the local spatial behaviors of the high-T_c cuprates, we show how the presence of an in-plane anisotropy has to be taken into account along with the mixed symmetry states of the order parameter components so as to explain the experimentally observed features of the high-T_c superconductors.

In the present work we have studied the properties of high temperature superconductors in the states of mixed symmetry of order parameter components, taking explicitly into account the effect of in-plane anisotropy. The anisotropy considered here is the electronic mass anisotropy ($\gamma = m_x/m_y$), which is introduced in the formulation in the form of an effective mass anisotropy tensor ($\mathbf{\Lambda}$). As an approximation, we have considered the effective electronic masses of the s and d-components to be the same (i.e. $m_s^* = m_d^* = m^*$), though in principle they are dependent on the corresponding Fermi surfaces. The properties have been studied in detail over the entire range of the magnetic field and wide range of temperature. This allows us to study the experimentally relevant intermediate field region ($H_{c1} \ll H \ll H_{c2}$) which shows an anomalous magnetic field dependence of the vortex lattice [26]. Also the studies are done for arbitrary values of the GL parameter κ_y and vortex lattice symmetry. Thus our study goes much beyond the limitations of the earlier studies on HTS using anisotropic GL theory [27]. In order to achieve this, we have extended the two-order parameter GL theory developed in a recent work [1] to take into account the effect of in-plane anisotropy. The numerical iteration technique developed in [1] enables us to solve the coupled nonlinear GL equations over the entire range of the applied magnetic field and temperature for arbitrary values of the GL parameter κ_y and vortex lattice symmetry.

Here we consider the vortex lattice axes to be parallel to the crystal symmetry axes of the lattice. The effect of the CuO chains and the orthorhombic distortion of the system has not been considered explicitly. As in the isotropic case, the pairing symmetry of the order parameters is considered to be $(d + is)$ with the corresponding phase difference between the order parameter components being $\pi/2$ [1]. We have carried out a detail study of the local spatial behavior such as the width and peak amplitude of the order parameters and magnetic field induction, the structure of the single vortex and vortex lattice structure, the shear modulus (c_{66}) of the vortex lattice etc and their variation with the mass anisotropy parameter γ. The effect of the mass anisotropy parameter γ on experimentally observable properties such as the vortex core radius, penetration depth of the magnetic field, superconducting current density, reversible magnetization etc, are studied in detail and the results are compared with the isotropic case and also with experimental data. In the following sections we will present the results obtained by our anisotropic two-order parameter GL theory, specially emphasizing the effect of in-plane mass anisotropy.

The paper is organized as follows, in section 2 we have discussed in detail the theoretical formalism, section 3 describes the numerical calculations involved in the work, the results obtained and their analysis. Finally section 4 is devoted to the conclusion drawn from the work done along with the future prospects.

2. Theoretical formalism

The two-dimensional average GL free energy density for high-T_c superconductors involving a mixed symmetry state of order parameter components with in-plane mass anisotropy can be

written as

$$f = \langle[\alpha_s\omega_s - \omega_d + \beta_1\omega_s^2 + \beta_2\omega_d^2 + \beta_3\omega_s\omega_d + 2\beta_4\cos(2\phi)\omega_s\omega_d + g_s + \omega_s\mathbf{Q}\mathbf{\Lambda}\mathbf{Q} + g_d + \omega_d\mathbf{Q}\mathbf{\Lambda}\mathbf{Q} + 2\epsilon_v[\cos(\phi)\{((\nabla_y\omega_s)(\nabla_y\omega_d) - (\nabla_x\omega_s)(\nabla_x\omega_d))/4\kappa_y^2(\omega_s\omega_d)^{1/2} + (Q_y^2 - Q_x^2)(\omega_s\omega_d)^{1/2}\} + \sin(\phi)\{[Q_y(\nabla_y\omega_s) - Q_x(\nabla_x\omega_s)](\omega_d/4\kappa_y^2\omega_s)^{1/2} - [Q_y(\nabla_y\omega_d) - Q_x(\nabla_x\omega_d)] \times (\omega_s/4\kappa_y^2\omega_d)^{1/2}\}] + (\nabla\times\mathbf{Q})^2]\rangle. \quad (1)$$

The above dimensionless equation is obtained by scaling with the parameter $|\alpha_d|^2/2\beta_2$. The parameters α_s and β_i ($i = 1, 2, 3, 4$) are positive quantities which are measured in terms of reduced units as $\alpha_s = \alpha_s/|\alpha_d|$ (where $\alpha_s = \alpha'(T - T_s)$ and $\alpha_d = \alpha'(T - T_d)$) with T_s and T_d being the critical temperatures for s and d-wave order parameter components respectively and $\beta_i = \beta_i/2\beta_2$. The parameter values are related to each other through various inequalities [1, 28, 29]. In the above equation, $\langle\ldots\rangle = \frac{1}{V}\int d\mathbf{r}\ldots$. denotes the spatial average, the dimensionless quantities, $s = \sqrt{\omega_s}\exp[i\phi_s]$, $d = \sqrt{\omega_d}\exp[i\phi_d]$ gives the superconducting order parameters with $\omega_d = |d|^2 \leqslant 1$ and $\omega_s = |s|^2 \leqslant 1$ and $g_i = (\nabla\omega_i\mathbf{\Lambda}\nabla\omega_i)/4\kappa_y^2\omega_i$ (with $i = s, d$). The gauge invariant quantity $\mathbf{Q}(x, y) = \mathbf{A}(x, y) - \nabla\phi(x, y)/\kappa_y$ gives the velocity of the superconducting electrons and $\mathbf{\Lambda}$ denotes the anisotropic mass tensor,

$$\mathbf{\Lambda} = \begin{pmatrix} m_y/m_x & 0 \\ 0 & 1 \end{pmatrix} \quad (2)$$

where the effective masses of the s and d-type electrons are considered to be the same i.e $m_s^* = m_d^* = m^*$. The magnetic field is applied along the z-axis and is thus defined as $\mathbf{B} = B\hat{z}$. The parameter $\epsilon_v = m_y/m_v$ (where m_v is defined as $\gamma_v = \hbar^2/2m_v^*$ [28]) serves as the coefficient of the mixed gradient coupling term and gives the strength of the admixture of the s-wave order parameter component. Thus, along with the variation of the strength of the in-plane mass anisotropy of the system through the parameter $\gamma = m_x/m_y$, we can also control the strength of the admixture of the s-wave order parameter component in the system. For $\gamma = 1.0$ ($m_x = m_y$) we obviously return to the isotropic system [1]. For $\epsilon_v = 0$, the pure d-wave state is realized. The major contribution of the s-wave order parameter component arises from the mixed gradient coupling term.

Minimizing the free energy density functional w.r.t the order parameters ω_d and ω_s and supervelocity $\mathbf{Q}$ as $\partial f/\partial\omega_s = \partial f/\partial\omega_d = 0$ and $\partial f/\partial\mathbf{Q} = 0$ we get the corresponding GL equations as

$$-\nabla\mathbf{\Lambda}\nabla\omega_s = 2\kappa_y^2[-\alpha_s\omega_s - 2\beta_1\omega_s^2 - \beta_3\omega_s\omega_d - 2\beta_4\cos(2\phi)\omega_s\omega_d - \omega_s\mathbf{Q}\mathbf{\Lambda}\mathbf{Q} - g_s - \cos(\phi)\epsilon_v \times (Q_y^2 - Q_x^2)(\omega_s\omega_d)^{1/2} - \cos(\phi)\epsilon_v[(\omega_s/\omega_d)^{1/2} \times (\nabla_x(\nabla_x\omega_d) - \nabla_y(\nabla_y\omega_d))/2\kappa_y^2] - \cos(\phi)\epsilon_v[(\omega_s/\omega_d)^{1/2} \times ((\nabla_y\omega_d)^2 - (\nabla_x\omega_d)^2)/4\kappa_y^2\omega_d] - 2\sin(\phi)\epsilon_v[(\omega_s/\omega_d)^{1/2} \times (Q_x(\nabla_x\omega_d) - Q_y(\nabla_y\omega_d))/2\kappa_y]] \quad (3)$$

$$-\nabla\mathbf{\Lambda}\nabla\omega_d = 2\kappa_y^2[\omega_d - 2\beta_2\omega_d^2 - \beta_3\omega_s\omega_d - 2\beta_4\cos(2\phi)\omega_s\omega_d - \omega_d\mathbf{Q}\mathbf{\Lambda}\mathbf{Q} - g_d - \cos(\phi)\epsilon_v(Q_y^2 - Q_x^2)(\omega_s\omega_d)^{1/2} - \cos(\phi)\epsilon_v[(\omega_d/\omega_s)^{1/2}(\nabla_x(\nabla_x\omega_s) - \nabla_y(\nabla_y\omega_s))/2\kappa_y^2] - \cos(\phi)\epsilon_v[(\omega_d/\omega_s)^{1/2}((\nabla_y\omega_s)^2 - (\nabla_x\omega_s)^2)/4\kappa_y^2\omega_s] - 2\sin(\phi)\epsilon_v[(\omega_d/\omega_s)^{1/2}(Q_y(\nabla_y\omega_s) - Q_x(\nabla_x\omega_s))/2\kappa_y]] \quad (4)$$

$$-\nabla^2\mathbf{Q} = -(\omega_s + \omega_d)\mathbf{\Lambda}\mathbf{Q} - \epsilon_v\{2\cos(\phi)(\omega_s\omega_d)^{1/2} \times (\hat{y}Q_y - \hat{x}Q_x) + \sin(\phi)[(\omega_d/4\kappa_y^2\omega_s)^{1/2} \times (\hat{y}(\nabla_y\omega_s) - \hat{x}(\nabla_x\omega_s)) - (\omega_s/4\kappa_y^2\omega_d)^{1/2}(\hat{y}(\nabla_y\omega_d) - \hat{x}(\nabla_x\omega_d))]\} \quad (5)$$

where $\phi = \phi_d - \phi_s$ is the phase difference between the d and s-wave order parameters and κ_y is the GL parameter.

The nonlinear coupled two-order parameter GL equations involving in-plane mass anisotropy are then solved over the entire range of applied magnetic field for arbitrary values of GL parameter κ_y and vortex lattice symmetry using a high precision numerical iteration technique as developed in [1]. In this numerical technique, the order parameters, magnetic field and the supervelocity of the electrons are first expressed in terms of the Fourier series [1, 30]. The corresponding Fourier coefficients $a_{\mathbf{K}}^s$, $a_{\mathbf{K}}^d$ and $b_{\mathbf{K}}$ are then determined numerically by iterating the three iteration equations obtained from the three GL equations. As mentioned in [1], two additional iteration equations are also used for a stable and faster convergence of the iteration process. The resulting five iteration equations for the anisotropic two-order parameter system are given as

$$a_{\mathbf{K}}^s := 2\langle[(\alpha_s - c_{1s})\omega_s + 2\beta_1\omega_s^2 + \beta_3\omega_s\omega_d + 2\beta_4\cos(2\phi)\omega_s\omega_d + \omega_s\mathbf{Q}\mathbf{\Lambda}\mathbf{Q} + g_s + \cos(\phi)\epsilon_v \times (Q_y^2 - Q_x^2)(\omega_s\omega_d)^{1/2} + (\omega_s/\omega_d)^{1/2} \times \{\cos(\phi)\epsilon_v[(\nabla_x(\nabla_x\omega_d) - \nabla_y(\nabla_y\omega_d))/2\kappa_y^2 + g_{dy} - g_{dx}] + 2\sin(\phi)\epsilon_v(Q_x\nabla_x\omega_d - Q_y\nabla_y\omega_d)/2\kappa_y\}] \times \cos(\mathbf{K}\cdot\mathbf{r})\rangle/(\mathbf{K}\mathbf{\Lambda}\mathbf{K}/2\kappa_y^2 + c_{1s}) \quad (6)$$

$$a_{\mathbf{K}}^s := a_{\mathbf{K}}^s \cdot \langle(c_{2s} - \alpha_s)\omega_s - \beta_3\omega_s\omega_d - 2\beta_4\cos(2\phi)\omega_s\omega_d - \omega_s\mathbf{Q}\mathbf{\Lambda}\mathbf{Q} - g_s - \cos(\phi)\epsilon_v(Q_y^2 - Q_x^2)(\omega_s\omega_d)^{1/2} - (\omega_s/\omega_d)^{1/2}\{\cos(\phi)\epsilon_v[(\nabla_x(\nabla_x\omega_d) - \nabla_y(\nabla_y\omega_d))/2\kappa_y^2 + g_{dy} - g_{dx}] + 2\sin(\phi)\epsilon_v(Q_x\nabla_x\omega_d - Q_y\nabla_y\omega_d)/2\kappa_y\}\rangle \times 1/(2\beta_1\langle\omega_s^2\rangle + c_{2s}\bar{\omega}_s) \quad (7)$$

$$a_{\mathbf{K}}^d := 2\langle[-(1 + c_{1d})\omega_d + 2\beta_2\omega_d^2 + \beta_3\omega_s\omega_d + 2\beta_4\cos(2\phi)\omega_s\omega_d + \omega_d\mathbf{Q}\mathbf{\Lambda}\mathbf{Q} + g_d + \cos(\phi)\epsilon_v \times (Q_y^2 - Q_x^2)(\omega_s\omega_d)^{1/2} + (\omega_d/\omega_s)^{1/2} \times \{\cos(\phi)\epsilon_v[(\nabla_x(\nabla_x\omega_s) - \nabla_y(\nabla_y\omega_s))/2\kappa_y^2 + g_{sy} - g_{sx}] - 2\sin(\phi)\epsilon_v(Q_x\nabla_x\omega_s - Q_y\nabla_y\omega_s)/2\kappa_y\}] \times \cos(\mathbf{K}\cdot\mathbf{r})\rangle/(\mathbf{K}\mathbf{\Lambda}\mathbf{K}/2\kappa_y^2 + c_{1d}) \quad (8)$$

$$a_{\mathbf{K}}^d := a_{\mathbf{K}}^d.\langle(c_{2d} + 1)\omega_d - \beta_3\omega_s\omega_d - 2\beta_4\cos(2\phi)\omega_s\omega_d - \omega_d\mathbf{Q}\mathbf{\Lambda}\mathbf{Q} - g_d - \cos(\phi)\epsilon_v(Q_y^2 - Q_x^2)(\omega_d\omega_s)^{1/2} - (\omega_d/\omega_s)^{1/2}\{\cos(\phi)\epsilon_v[(\nabla_x(\nabla_x\omega_s) - \nabla_y(\nabla_y\omega_s))/2\kappa_y^2 + g_{sy} - g_{sx}] - 2\sin(\phi)\epsilon_v(Q_x\nabla_x\omega_s - Q_y\nabla_y\omega_s)/2\kappa_y\}\rangle/(2\beta_2\langle\omega_d^2\rangle + c_{2d}\bar{\omega}_d) \quad (9)$$

$$
\begin{aligned}
b_{\mathbf{K}} := 2\langle[&-\omega_{\mathrm{d}}B - P_{\mathrm{d}} + (\bar{\omega}_{\mathrm{s}} + \bar{\omega}_{\mathrm{d}})(B - \bar{B}) - (\omega_{\mathrm{s}}B + P_{\mathrm{s}}) \\
&- [2\cos(\phi)\epsilon_v\{(\omega_{\mathrm{s}}\omega_{\mathrm{d}})^{1/2}(\nabla_x Q_y + \gamma\nabla_y Q_x) \\
&+ (1/2)(\omega_{\mathrm{s}}/\omega_{\mathrm{d}})^{1/2}[Q_y\nabla_x\omega_{\mathrm{d}} + Q_x\gamma\nabla_y\omega_{\mathrm{d}}] \\
&+ (1/2)(\omega_{\mathrm{d}}/\omega_{\mathrm{s}})^{1/2}[Q_y\nabla_x\omega_{\mathrm{s}} + Q_x\gamma\nabla_y\omega_{\mathrm{s}}]\}] \\
&+ (\sin(\phi)/2\kappa_y)\epsilon_v\{(1/2)((\nabla_y\omega_{\mathrm{s}})(\nabla_x\omega_{\mathrm{d}}))(\omega_{\mathrm{s}}\omega_{\mathrm{d}})^{-1/2} \\
&+ (1/2)((\nabla_x\omega_{\mathrm{s}})\gamma(\nabla_y\omega_{\mathrm{d}}))(\omega_{\mathrm{s}}\omega_{\mathrm{d}})^{-1/2} \\
&- (\omega_{\mathrm{s}}/\omega_{\mathrm{d}})^{1/2}(\nabla_x(\nabla_y\omega_{\mathrm{d}}) + \nabla_y\gamma(\nabla_x\omega_{\mathrm{d}}) \\
&- (1/2)(\nabla_y\omega_{\mathrm{d}})(\nabla_x\omega_{\mathrm{d}})/\omega_{\mathrm{d}} - (1/2)(\nabla_x\omega_{\mathrm{d}})\gamma(\nabla_y\omega_{\mathrm{d}})/\omega_{\mathrm{d}}) \\
&+ (\omega_{\mathrm{d}}/\omega_{\mathrm{s}})^{1/2}(\nabla_x(\nabla_y\omega_{\mathrm{s}}) + \nabla_y\gamma(\nabla_x\omega_{\mathrm{s}}) \\
&- (1/2)((\nabla_y\omega_{\mathrm{s}})(\nabla_x\omega_{\mathrm{s}}))/\omega_{\mathrm{s}} - (1/2)((\nabla_x\omega_{\mathrm{s}})\gamma \\
&\times(\nabla_y\omega_{\mathrm{s}}))/\omega_{\mathrm{s}}) - (1/2)((\nabla_y\omega_{\mathrm{d}})(\nabla_x\omega_{\mathrm{s}}))(\omega_{\mathrm{s}}\omega_{\mathrm{d}})^{-1/2} \\
&- (1/2)((\nabla_x\omega_{\mathrm{d}})\gamma(\nabla_y\omega_{\mathrm{s}}))(\omega_{\mathrm{s}}\omega_{\mathrm{d}})^{-1/2}\}] \\
&\times \cos(\mathbf{K}\cdot\mathbf{r})\rangle/[(m_x/m_y)\mathbf{K}\mathbf{\Lambda}\mathbf{K} + (\bar{\omega}_{\mathrm{d}} + \bar{\omega}_{\mathrm{s}})\}] \qquad (10)
\end{aligned}
$$

where $P_i = (\nabla\omega_i \times \mathbf{Q})\cdot\hat{z}$ and $g_{ij} = (\nabla_j\omega_i)^2/4\kappa_y^2\omega_i$ (with $i = \mathrm{s}, \mathrm{d}$ and $j = x, y$). The convergence and stability of the iteration method can be enhanced by the choice of the constants cs. While the value of the constant $c_{1\mathrm{s}}$ is determined by an empirical relation $c_{1\mathrm{s}} \approx \frac{8\times10^3}{(6/b)+50(1-b/4)}$, the constant $c_{2\mathrm{s}}$ and $c_{2\mathrm{d}}$ are small positive quantities while $c_{1\mathrm{d}}$ is chosen to be 1. The iteration is started with the Abrikosov value for the d-wave order parameter component ($a^{\mathrm{d}}_{\mathbf{K}} = a^{\mathrm{A}}_{\mathbf{K}}$), while for the s-wave component, the initial value is chosen to be one order of magnitude smaller than that of the d-wave. For a given set of parameters, equations (6)–(10) are iterated till the solution remains constant up to 15 digits. The solution of the coupled nonlinear GL equations are thus obtained for the two-order parameter GL theory in the presence of in-plane mass anisotropy.

3. Numerical calculations, results and discussions

As mentioned above, the nonlinear coupled GL equations involving two-order parameter components, magnetic field and in-plane mass anisotropy characterized by the parameter γ are solved by using a numerical iteration technique. The various properties of the high-T_{c} material involving mixed symmetry states of order parameter components are computed and the effect of the presence of in-plane mass anisotropy on these properties are studied for different values of the magnetic induction parameter b ($=\bar{B}/B_{\mathrm{c2}}$) and temperature.

To obtain the vortex lattice structure, we begin by minimizing the free energy density $f(x_2 = x_1/2, y_2)$ w.r.t the vortex lattice parameter y_2. The position of the vortices in the flux line lattice is given by $\mathbf{R} = \mathbf{R}_{mn} = (mx_1 + nx_2, ny_2)$ (m and n are integers). For a triangular vortex lattice, one has $x_2 = x_1/2$, $y_2 = x_1\sqrt{3}/2$, while for the square vortex lattice $x_2 = 0$, $y_2 = x_1$. The lattice parameter y_2 thus characterizes the structure of the vortex lattice corresponding to the most stable configuration (minimum free energy density) for a particular choice of other parameters in the model.

Figure 1 shows the minimization of the free energy density with the lattice parameter y_2/x_1 ($x_1 = 1.0$). The magnetic induction parameter $b = \bar{B}/B_{\mathrm{c2}}$ is chosen to be $b = 0.04$, which corresponds to the experimental applied field of $H = 5$ T [24]. The GL parameter κ_y, is chosen to be 72 as observed experimentally for high-T_{c} cuprate $YBa_2Cu_3O_{7-\delta}$ [26]. The value of the mass anisotropy parameter γ is taken as 2.4, as observed experimentally for high-T_{c} cuprate $YBa_2Cu_3O_{7-\delta}$ [23]. The value of the parameter ϵ_v is chosen as 0.1 (as in [1] where we have shown that the best fit to the experimental data of high-T_{c} cuprate $YBa_2Cu_3O_{7-\delta}$ are obtained for $\epsilon_v = 0.1$). This is also consistent with the theoretical work carried out by Feder *et al* [31], where they have studied the d-wave superconductor involving an admixture of the s-wave order parameter component by using two different models namely the extended Hubbard model and the antiferromagnetic van Hove model. They have found that both the models suggest a gradient coupling coefficient of $\epsilon_v = \gamma_v/\gamma_{\mathrm{d}} \approx 0.1$–$0.4$. The result had also been found to be consistent with experimental observations [24, 25] for YBCO flux line lattices. For the anisotropic system, we have found that the value of y_2 which corresponds to the minimum of free energy remains same for all values of the coefficient ϵ_v between 0.1 and 0.4. This is shown in the inset of figure 1, where we have plotted the variation of free energy with lattice parameter y_2 for different values of the coupling parameter ϵ_v and $\gamma = 2.4$. In the remainder of this paper we take the value of the mixed gradient coupling parameter $\epsilon_v = 0.1$. As shown in figure 1, the minimum free energy is obtained for $y_2 = 0.55$ which corresponds to the oblique lattice. For this value of $y_2 = 0.55$, the angle between the primitive axes is $\beta \approx 84.5°$ which is quite close to the experimentally determined value of $\beta = 77° \pm 5°$ [24, 25] for the applied magnetic field of $H = 5$ T ($b = 0.04$). The difference between the experimental and theoretical results can be attributed to the fact that in the present work the chain structure of the high-T_{c} cuprates as well as the resulting orthorhombic distortion of the system has not been taken into account explicitly. It is appropriate to mention here that for the isotropic case, as studied earlier by us [1] the value

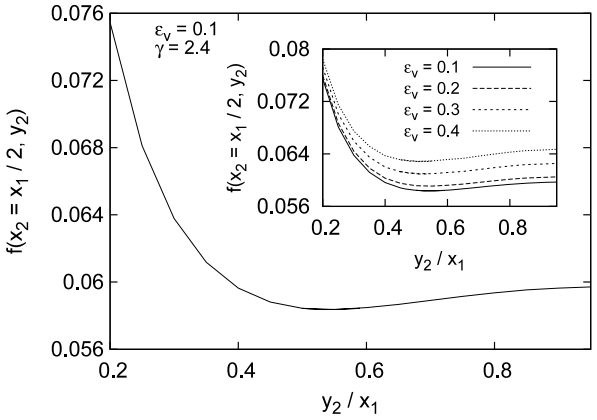

Figure 1. Variation of free energy density with lattice parameter y_2 ($x_1 = 1.0$) for mass anisotropy parameter $\gamma = 2.4$. Other parameter values used are, $\alpha_{\mathrm{s}}/|\alpha_{\mathrm{d}}| = 0.5$, $\beta_1/2\beta_2 = \beta_3/2\beta_2 = 1.0$, $\beta_4/2\beta_2 = 0.5$, GL parameter $\kappa_y = 72$ and the phase difference between the d and s-wave order parameter components is $\phi = \phi_{\mathrm{d}} - \phi_{\mathrm{s}} = \pi/2$. The inset shows the free energy density minimization for different values of the mixed gradient coupling parameter ϵ_v with $\gamma = 2.4$.

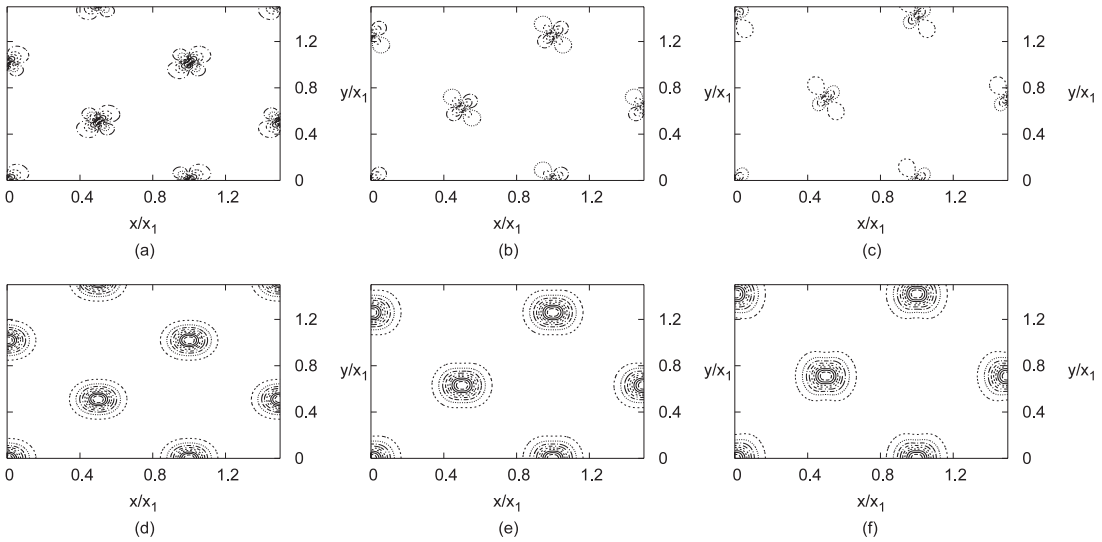

Figure 2. Contour plots of the order parameter components for different values of the mass anisotropy parameter γ. (a)–(c) corresponds to the s-wave order parameter component $\omega_s(x, y)$ while (d)–(f) corresponds to the d-wave order parameter component $\omega_d(x, y)$ for $\gamma = 2.0, 3.0, 4.0$, respectively. Other parameter values used are the same as in figure 1.

of the angle is $\beta \approx 97.3°$ which is far from the experimental value of $\beta \approx 77° \pm 5°$. The observation justifies the fact that the mixed symmetry scenario alone cannot explain all the observed features of the high-T_c superconductors and the presence of in-plane anisotropy has to be taken into consideration.

The change in the mass anisotropy parameter γ results in a change in the vortex lattice structure, though the lattice in general remains oblique. Figure 2 shows the contour plots of $\omega_s(x, y)$ and $\omega_d(x, y)$ for different values of γ. The vortex lattice structure remains in general oblique as mentioned above, with the exact shape being dependent upon γ. We have found that on varying γ as 2.0, 3.0, 4.0, 5.0, 6.0 etc (for $\epsilon_v = 0.1$), the stable lattice configuration is obtained for $y_2 = 0.51, 0.63, 0.71, 0.82, 0.86$ respectively.

A closer observation of the single vortex structure indicates a four-fold structure of the s-wave order parameter component $\omega_s(x, y)$, characteristic of the mixed symmetry scenario, with the exact shape being dependent on the mass anisotropy parameter γ. The d-wave order parameter component $\omega_d(x, y)$ also shows dependence on the mass anisotropy parameter γ, which leads to an elongated shape of its vortex structure, in agreement with experiment [25]. The ratio of the axes of this elliptic vortex structure is found to be $\approx$1.4 for the experimental applied field of $H = 5$ T ($b = 0.04$). The observation is in accordance with the coherence length anisotropy determined by STM measurements of YBCO [25].

Before concluding the section we would like to mention that for very low magnetic fields (i.e. for the single vortex solution) the structure of the s-wave vortex changes from four-fold to two-fold symmetry. The d-wave solution also shows tapering at both ends indicating a two-fold symmetry. Such a two-fold symmetric state has also been observed by Xu *et al* [27] in their study of anisotropic d-wave superconductors. It should be mentioned that the two-fold symmetry is not observed for the isotropic case [1], thereby suggesting that its origin may be due to anisotropy in the system. The effect of anisotropy becomes clearer from the observation that for any particular applied magnetic field, the two-fold symmetry of the single vortex structure gets enhanced with an increase in mass anisotropy parameter γ. Figure 3 shows such a situation where we have plotted the single vortex solution of the s and d-wave order parameter components for three different values of in-plane anisotropy parameter γ.

The effect of the presence of in-plane mass anisotropy in the system is also observed in the magnetic field profile $B(x, y)$ as shown in figure 4. The flux line lattice is again oblique with the exact shape being determined by the value of the mass anisotropy parameter γ.

We now calculate the local spatial behaviors of the order parameters and magnetic field profiles, which are important quantities since they give an insight to the two length scales of the superconducting systems, namely the vortex core radius and the penetration depth [1]. In figure 5 we have shown the variation of the combined vortex core radius (calculated along the x-direction and denoted by $r_x(b)$) of the d and s-wave order parameter components for arbitrary values of the magnetic field induction b. For a given value of the mass anisotropy parameter γ the vortex core radius decreases with an increase in the magnetic field induction indicating the shrinkage of the vortex core at higher magnetic fields. This is also in agreement with the experimental observation for high-T_c superconducting cuprates, as shown in inset (a) of the figure [32, 33]. Inset (b) shows the variation of vortex core radius ($r_y(b)$), calculated along the y-direction, with magnetic field induction b. As can be seen from the figure, the vortex core radius measured along the y-direction has a larger magnitude than that measured along the x-direction, thereby showing it is anisotropic.

Figure 6 shows the variation of the peak amplitude of $\omega_d(x, 0)$ and $\omega_s(x, 0)$ with the magnetic field induction b. It is seen that for an increase in the anisotropy parameter γ, the peak amplitude of the order parameter components increases

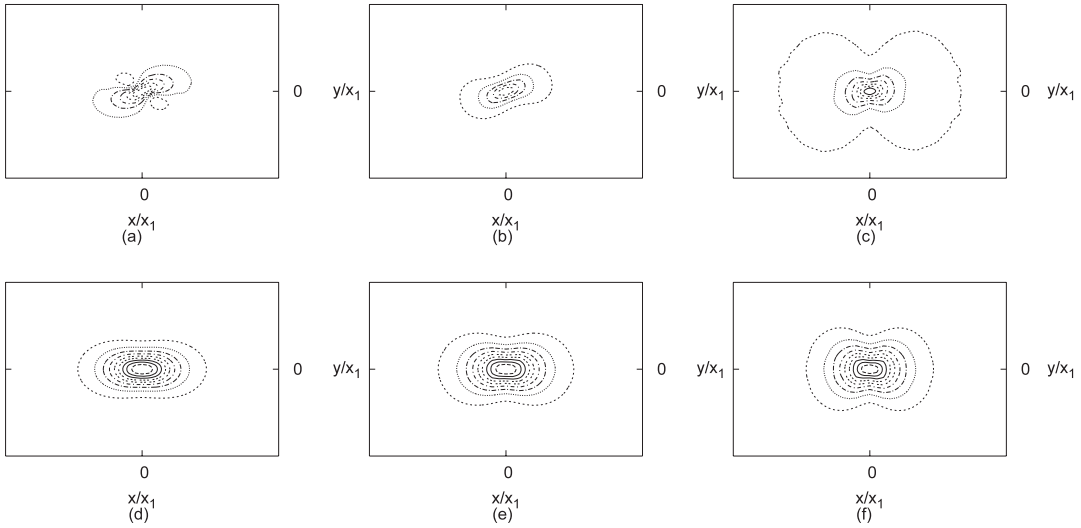

Figure 3. Single vortex solution for the order parameter components for different values of mass anisotropy parameter γ and magnetic field induction $b = 0.01$. (a)–(c) corresponds to $\omega_s(x, y)$, while (d)–(f) corresponds to $\omega_d(x, y)$ for $\gamma = 3.0, 5.0, 8.0$, respectively. Other parameter values are the same as figure 1. With an increase in the mass anisotropy parameter γ the vortex structure becomes more and more two-fold symmetric.

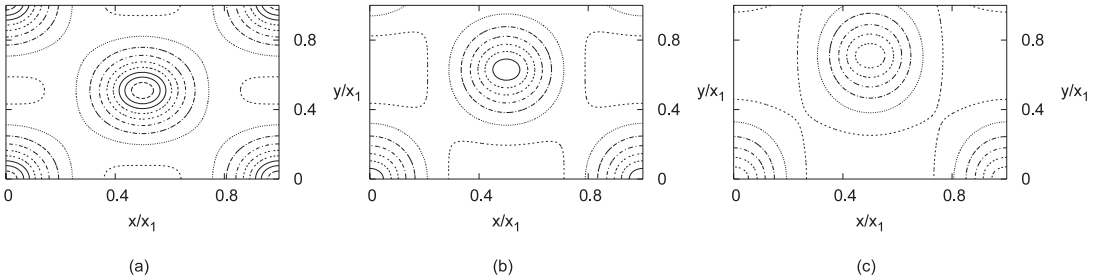

Figure 4. Contour plots of magnetic field $B(x, y)$ for mass anisotropy parameter $\gamma = 2.0, 3.0, 4.0$, respectively. Other parameter values are the same as in figure 1.

for both the order parameter components. However, as in the isotropic case [1], the overall amplitude of the s-wave order parameter component remains very small as compared to the d-wave order parameter component. Figure 7 shows the temperature dependence of the vortex core radius calculated along the x-direction for various values of the mass anisotropy parameter γ. For a given value of the parameter γ, the vortex core size increases with an increase in temperature. The inset of the figure shows the temperature dependence of the vortex core radius calculated along the y-direction for different values of the mass anisotropy parameter γ. The magnitude of the core radius measured along the y-direction is again found to be more than that along the x-direction.

Figure 8 shows the temperature dependence of the calculated vortex core radius (along y-direction) for mass anisotropy parameter $\gamma = 2.4$ and magnetic field induction $b = 0.004$ ($H = 0.5$ T) and comparison with the experimental data for high-T_c cuprate $YBa_2Cu_3O_{7-\delta}$ [33]. The match between the experimental and theoretical results is found to be fairly good. Figure 9 shows the variation of the width of the magnetic field profile $B(x, 0)$ with the magnetic field induction b for different values of the mass anisotropy parameter γ. As mentioned before, the width of the magnetic field profile gives a measure of the penetration depth of the system and it can be seen from the figure that for a given value of the mass anisotropy parameter γ, the penetration depth increases with an increase in the magnetic field induction b as expected. This is in agreement with the experimentally observed behavior of $YBa_2Cu_3O_{7-\delta}$ (inset (a)) [33]. Similar behavior is seen for $B(0, y)$ (inset (b)). Figure 10 shows the temperature dependence of the penetration depth of the magnetic field profile $B(x, 0)$ (calculated along the x-direction and denoted as $\lambda_x(T)$) for different values of the mass anisotropy parameter γ. For a given value of the parameter γ, the penetration depth increases with an increase in the temperature, an observation in agreement with the experimental results [34]. The inset of the figure shows the temperature dependence of penetration depth of the magnetic field profile $B(0, y)$ calculated along the y-direction and denoted as $\lambda_y(T)$. Figure 11 shows the temperature dependence of the penetration depth calculated for the mass anisotropy parameter $\gamma = 2.4$ and magnetic field induction $b = 0.004$ ($H = 0.5$ T) and compared with the experimental data for $YBa_2Cu_3O_{7-\delta}$ [34]. The match between the results has been found to be fairly good. The theoretical calculations in this case were carried out along the y-direction. As seen in figures 9 and 10, the penetration

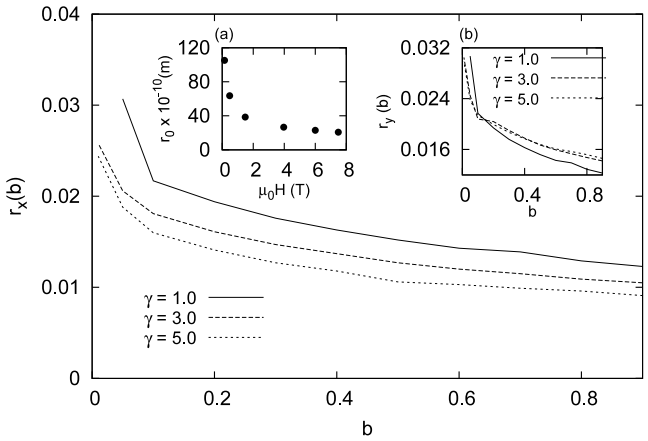

Figure 5. Variation of the vortex core radius ($r_x(b)$) calculated along the x-direction with magnetic field induction b for different values of the mass anisotropy parameter γ. Other parameters are the same as in figure 1. Inset (a) shows the experimental data for the magnetic field dependence of the vortex core radius of the high-T_c superconductor $YBa_2Cu_3O_{7-\delta}$ [33]. Inset (b) of the figure shows the magnetic field dependence of the vortex core radius ($r_y(b)$) calculated along the y-direction by our theoretical model for different values of the mass anisotropy parameter γ.

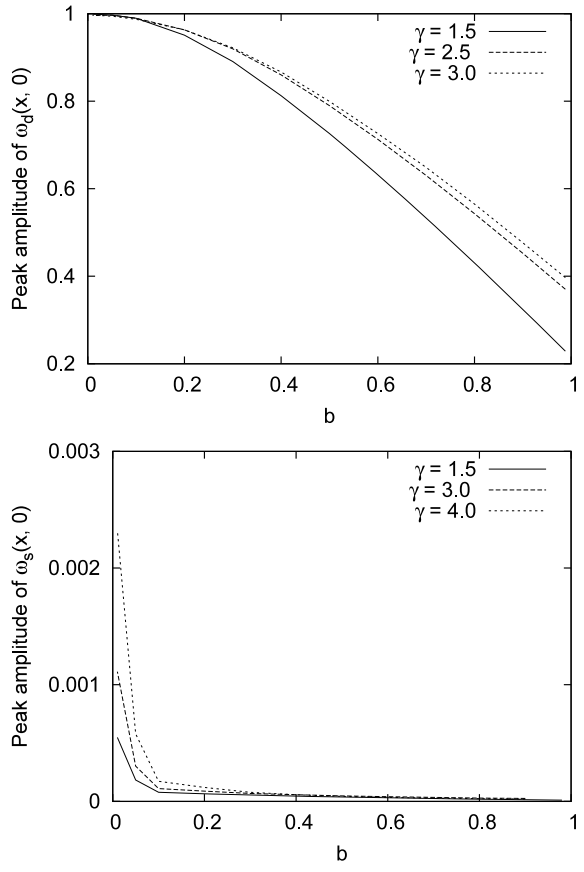

Figure 6. Variation of peak amplitude of the order parameters $\omega_d(x, 0)$ and $\omega_s(x, 0)$ with magnetic field induction b for different values of the mass anisotropy parameter γ. Other parameters are the same as figure 1.

depth measured along the y-direction ($\lambda_y(T)$) exceeds that along the x-direction ($\lambda_x(T)$) indicating an anisotropy in the penetration depth. This observation indicates a larger

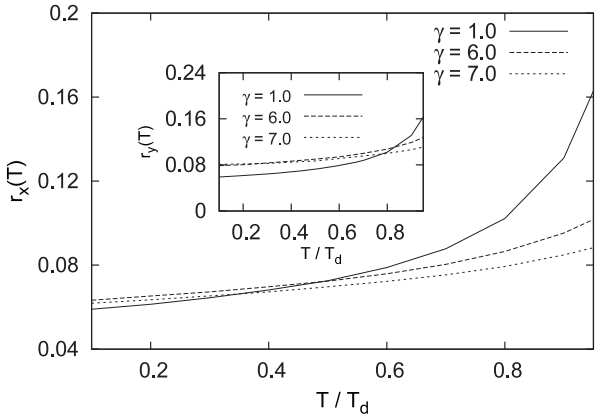

Figure 7. Variation of the vortex core radius ($r_x(T)$) calculated along the x-direction, with temperature T/T_d, for different values of the mass anisotropy parameter γ. The inset of the figure shows the same quantity calculated along the y-direction. Other parameters are the same as in figure 1, with $T/T_s = 0.5$.

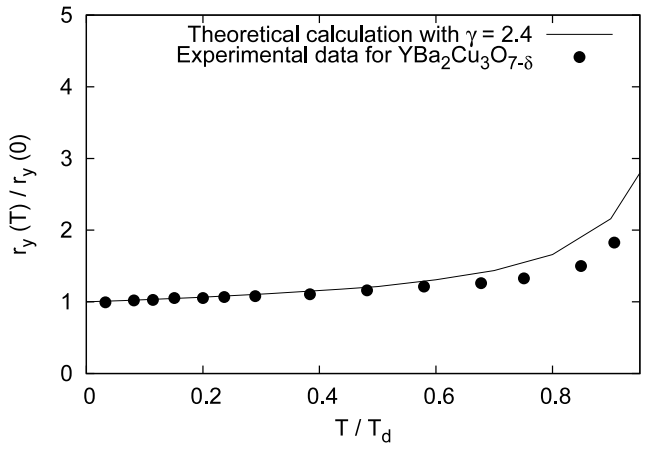

Figure 8. Temperature dependence of the vortex core radius. The solid line gives the results calculated theoretically by our anisotropic two-order parameter model for the in-plane anisotropy parameter $\gamma = 2.4$ and magnetic field induction $b = 0.004$ ($H = 0.5$ T). Other parameter values used for the theoretical calculation are the same as in figure 1 with $T/T_s = 0.5$. The dots give the experimental data for high-T_c cuprate $YBa_2Cu_3O_{7-\delta}$ [33].

supercurrent response along the y-direction as compared to that along the x-direction.

Figure 12 shows the current density profile $|j(x, 0)|$ plotted along the x-direction for different values of the magnetic field induction b. It can be seen that the magnitude of the current density increases with a decrease in the magnetic field induction b. The position of the maxima of current also gives a measure of the core radius [33]. This is shown in the inset of figure 12. In-plane mass anisotropy also shows a pronounced effect on the current profile. Figure 13 shows the variation of the current profile with mass anisotropy parameter γ. Figure 14 shows the plots of the components of average current densities along the x and y-directions for the experimentally relevant magnetic field induction of $b = 0.004$ ($H = 0.5$ T). The difference in their magnitude at any temperature shows the effect of the anisotropy. In

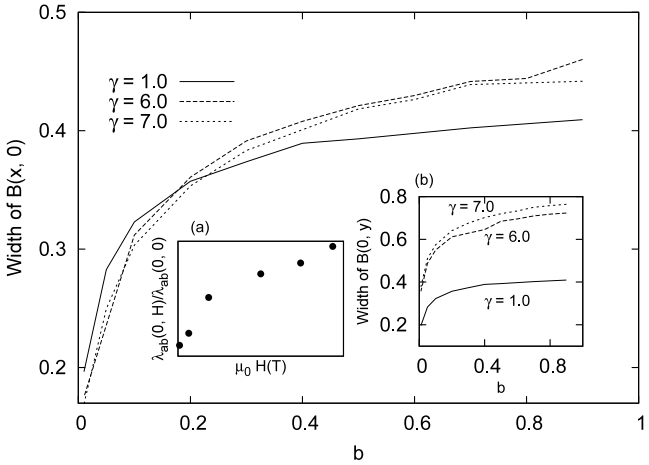

Figure 9. Variation of the width of the magnetic field profile ($B(x, 0)$) calculated along the x-direction with magnetic field induction b for different values of the mass anisotropy parameter γ. Inset (b) shows the width for magnetic field profile ($B(0, y)$). Other parameters are the same as in figure 1. Inset (a) shows the experimental data for the magnetic field dependence of the penetration depth of the high-T_c superconductor $YBa_2Cu_3O_{7-\delta}$ [33].

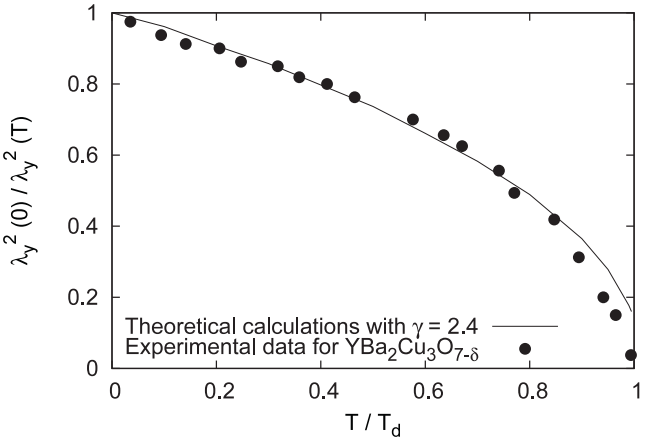

Figure 11. Temperature dependence of the penetration depth. The solid line gives the results calculated theoretically by our anisotropic two-order parameter model for the in-plane anisotropy parameter $\gamma = 2.4$ and magnetic field induction $b = 0.004$ ($H = 0.5$ T). Other parameter values used for the theoretical calculation are the same as in figure 1 with $T/T_s = 0.5$. The dots give the experimental data for the high-T_c cuprate $YBa_2Cu_3O_{7-\delta}$ [34].

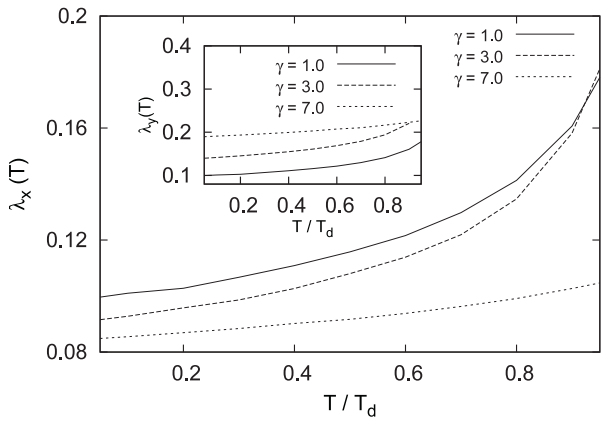

Figure 10. Variation of the penetration depth ($\lambda_x(T)$) calculated along the x-direction, with temperature T/T_d for different values of the mass anisotropy parameter γ. The inset of the figure shows the same quantity calculated along the y-direction. Other parameters are the same as in figure 1, with $T/T_s = 0.5$.

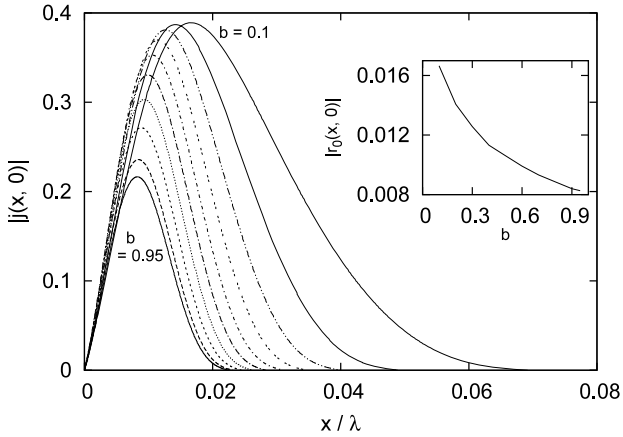

Figure 12. Supercurrent profile for different values of the magnetic field induction ($b = 0.95, 0.9, 0.8, 0.7, 0.6, 0.5, 0.4, 0.3, 0.2, 0.1$) for a particular value of the mass anisotropy parameter $\gamma = 3.0$. Other parameters are the same as in figure 1. The inset shows the magnetic field dependence of the vortex core radius as calculated from the supercurrent profile.

figure 15 we have plotted the calculated current density with the experimental data for YBCO [35]. Since the experiment is at zero applied magnetic field we have carried out our calculations for a very small magnetic field induction $b = 0.004$ ($H = 0.5$ T). The behavior is qualitatively the same, the exact numerical values cannot however be compared since the experimental data is for thin films and we have also not taken the pinning mechanism into consideration.

Another quantity which we can calculate from our model and compare with experiment is the reversible magnetization. The reversible magnetization is defined as, $M = \bar{B} - B_a$, where B_a is the applied magnetic field and can be defined as $B_a = 4\pi(\partial f/\partial \bar{B})$. However, as we have shown earlier, the cumbersome process of taking the numerical derivative can be avoided by making use of the virial theorem [36]. We use the same method to calculate the reversible magnetization for the anisotropic case also. Figure 16 shows the comparison between the calculated reversible magnetization for $\gamma = 2.4$ with experimental data for $YBa_2Cu_3O_{7-\delta}$ [26]. As can be seen from the figure, the match between the experimental and the calculated results is fairly good. The variation of the reversible magnetization with increasing anisotropy shows an almost similar behavior for all magnetic induction parameter values b except at lower induction where the difference can be seen more clearly. This is shown in the inset of figure 16.

We next consider the shear modulus of the vortex lattice (c_{66}), which is a numerically computable quantity, and gives the stiffness (hardness) of the vortex lattice against thermal instabilities. For the anisotropic case the shear modulus, which depends upon the difference of the free energy density between

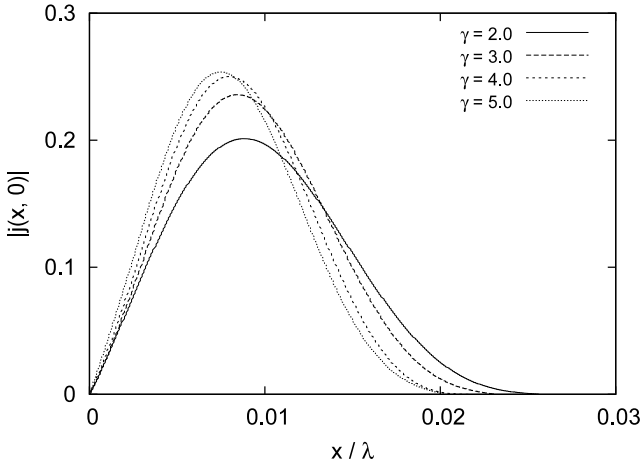

Figure 13. Supercurrent profile for different values of the mass anisotropy parameter γ ($\gamma = 2.0, 3.0, 4.0, 5.0$) for the magnetic field induction $b = 0.5$. Other parameters are the same as in figure 1.

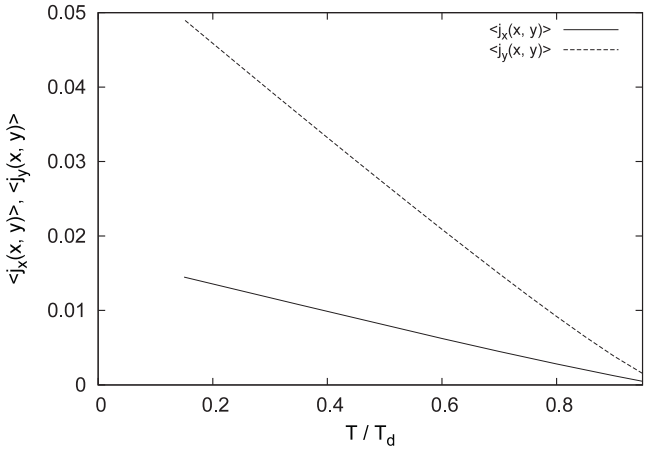

Figure 14. Temperature dependence of the different components of the superconducting current density calculated for the in-plane mass anisotropy parameter $\gamma = 2.4$. The magnetic field induction is $b = 0.004$ and the other parameters are the same as in figure 1, with $T/T_s = 0.5$.

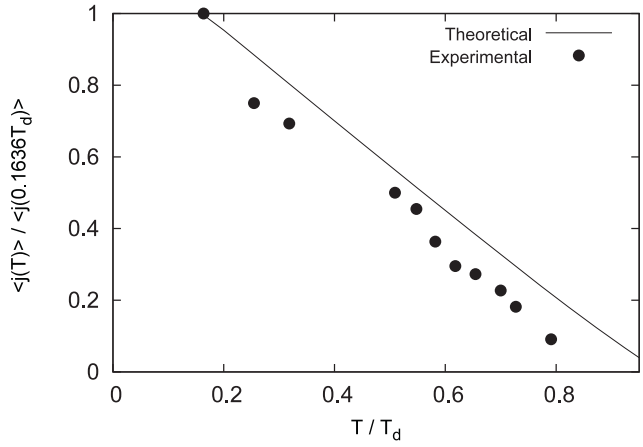

Figure 15. Comparison of the temperature dependence of current density calculated by our anisotropic two-order parameter GL theory for mass anisotropy parameter $\gamma = 2.4$ and $b = 0.004$ with the experimental data for a $YBa_2Cu_3O_{7-\delta}$ thin film [35].

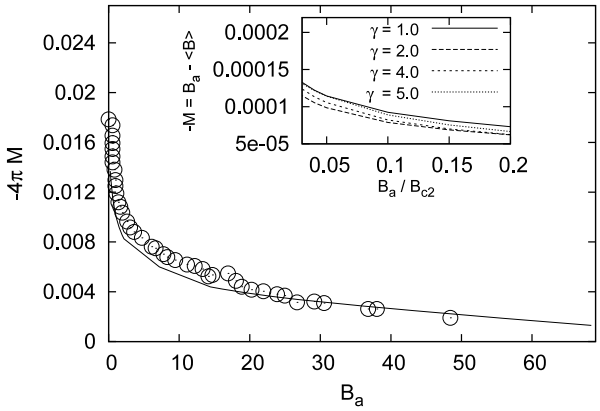

Figure 16. Comparison of the reversible magnetization results calculated by our anisotropic two-order parameter GL theory for mass anisotropy parameter $\gamma = 2.4$ with the corresponding experimental data for the high-T_c cuprate $YBa_2Cu_3O_{7-\delta}$ [26]. The inset of the figure shows the variation of reversible magnetization for different values of mass anisotropy parameter γ.

a rectangular and an oblique flux line lattice, is given by the relation [37]

$$c_{66} = 2\pi^2[y_2(\gamma)/x_1]^2 \times [f(x_2 = 0, y_2(\gamma)) - f(x_2 = x_1/2, y_2(\gamma))] \quad (11)$$

where $y_2(\gamma)$ denotes the anisotropy parameter dependent value of unit cell height which corresponds to the minimum free energy density for the vortex lattice of a given symmetry. Figure 17 shows the variation of the peak amplitude of the shear modulus of the vortex lattice, while figure 18 shows the variation of the peak position (b_{peak}), i.e. the value of the magnetic induction b at which the c_{66} value becomes maximum, with the mass anisotropy parameter γ. As has been mentioned in [1] the peak amplitude and the peak position are important quantities, the peak amplitude determines the hardness i.e. the stability of the vortex lattice, while the peak position (b_{peak}) denotes the magnetic field induction at the peak amplitude. With an increase of mass anisotropy parameter γ, the peak amplitude increases whereas the peak position decreases. The figures show that the presence of in-plane mass anisotropy in the system tends to harden the vortex lattice. In other words, the in-plane mass anisotropy does not favor the melting of the flux line lattice, an observation contrary to the popular belief that the presence of mass anisotropy leads to the softening of the vortex lattice. This is an important observation and in order to correlate it with the experimental results, experiments which can probe the melting of the vortex lattice as a function of increasing in-plane anisotropy should be carried out. Here it must be mentioned that for an isotropic two-order parameter system [1], an increase in the admixture of the s-wave order parameter component in the system decreases the shear modulus of the vortex lattice, indicating that melting is favored in high-T_c superconducting cuprates. However, once in-plane anisotropy is introduced into the system, the effect of the admixture of s-wave order parameter component in the system is suppressed by the effect of in-plane anisotropy and the flux line lattice gets hardened with increasing anisotropy, thus resisting its melting.

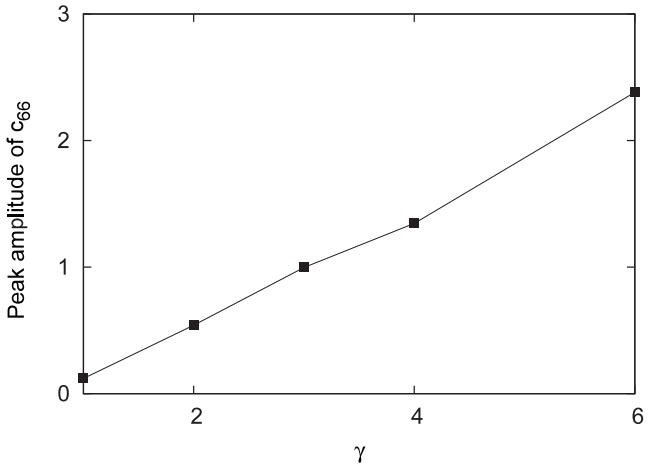

Figure 17. Variation of the peak amplitude of the shear modulus (c_{66}) of the vortex lattice with different values of the mass anisotropy parameter γ. Other parameters are the same as in figure 1.

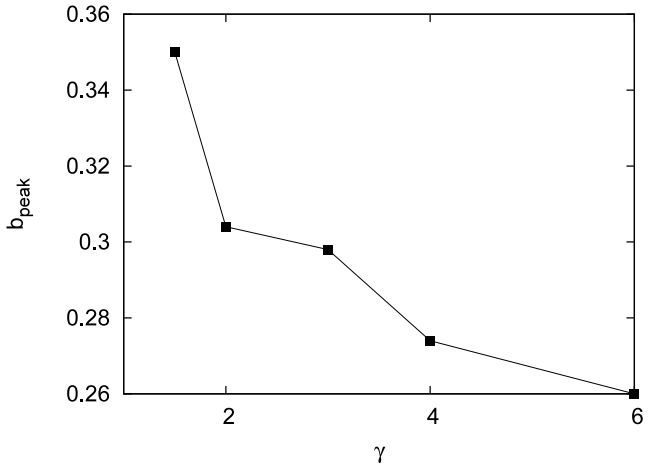

Figure 18. Variation of the peak position (b_{peak}) of c_{66} with different values of the mass anisotropy parameter γ. Other parameters are the same as in figure 1.

The effect of temperature on the shear modulus of the vortex lattice has also been studied for different values of the mass anisotropy parameter (γ) and the results are shown in figure 19. As can be seen from the figure, an increase in the mass anisotropy enhances the shear modulus of the vortex lattice. For any particular value of the mass anisotropy parameter γ, the shear modulus of the vortex lattice decreases with an increase in the temperature indicating that the melting of the vortex lattice is favored at high temperature.

4. Conclusion

In conclusion, we have presented a detailed systematic study of the properties of anisotropic high temperature superconductors in the states of mixed symmetry of order parameter components. The study is carried out in the framework of an anisotropic two-order parameter GL theory and the effect of in-plane anisotropy is taken into account by

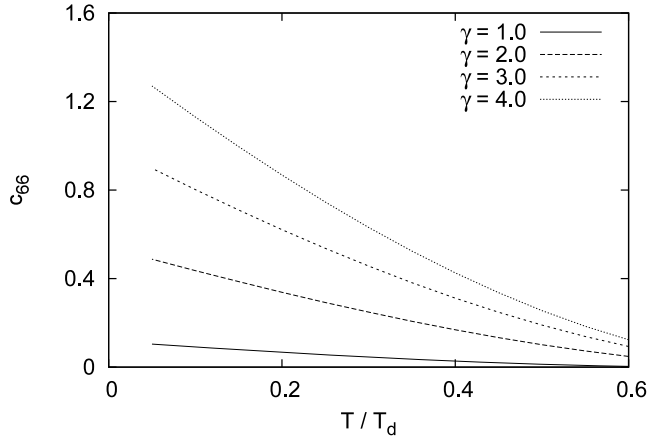

Figure 19. Temperature dependence of the shear modulus (c_{66}) of the vortex lattice for different values of the mass anisotropy parameter γ with magnetic field induction $b = 0.3$. Other parameters are the same as in figure 1.

an effective mass approximation, which is characterized by the mass anisotropy parameter γ. The main focus of the study has been on the effect of the in-plane mass anisotropy parameter γ on the various properties of the high-T_c superconductors, over the entire range of magnetic field induction b and a wide range of temperature, for arbitrary values of the GL parameter κ_y and vortex lattice symmetry. The results show the marked effect of the presence of in-plane mass anisotropy when compared to those obtained in the isotropic case [1]. We have found that the presence of in-plane anisotropy gives rise to an oblique vortex lattice structure with the angle between the primitive axes of the lattice being $\beta \approx 85°$ for the experimentally determined mass anisotropy parameter $\gamma = 2.4$. The result is in good agreement with the experimental observations of $\beta \approx 77° \pm 5°$ [24, 25]. The small difference in the experimental and theoretically calculated results arises due to the fact that in the present work the chain structure and the resulting orthorhombic distortion of the system has not been taken into account explicitly. Moreover, the three-dimensional nature of the system has not been taken into consideration. The anisotropy in the coherence length of the system, as obtained from the structure of the vortices (d-wave), amounts to a value of ≈1.5, which again satisfies the STM results of YBCO [25]. For lower values of the magnetic field induction b (i.e. for the single vortex limit) the structure of the vortices of the s-wave order parameter component changes from four-fold to two-fold. For very low induction b, the d-wave order parameter component also shows two-fold symmetry. Such an observation has not been found in the isotropic case and can thus be attributed to the presence of in-plane anisotropy in the system. It must be noted that such a two-fold symmetry of the vortex structure has been observed by Xu *et al* [27] also. However, in their work they have explicitly taken into account the presence of orthorhombic distortion in the system. In the present work we have shown that such a two-fold symmetry will arise from the anisotropic effect due to the effective mass approximation, even in the absence of an explicit orthorhombic distortion term being taken into account in the formalism.

We have also calculated other relevant properties of the high-T_c superconductor in the states of mixed symmetry, namely the local spatial behaviors such as, the vortex core radius and penetration depth of the system, the reversible magnetization, the shear modulus of the vortex lattice, the superconducting current etc, and have shown the effect of in-plane mass anisotropy on these properties. We have compared our results with those obtained from the isotropic model and the effect of the in-plane anisotropy is clearly very evident in each case. Comparison of the results with experimental data for the high-T_c cuprate $YBa_2Cu_3O_{7-\delta}$ shows fairly good agreement. The shear modulus of the vortex lattice and its variation with the magnetic field induction and temperature shows that an increase in the in-plane mass anisotropy in the system does not favor melting of the vortex lattice. More experiments on the melting of the vortex lattice are required to verify this observation.

Before we conclude, we would like to mention that in the present work we have not considered the effect of thermodynamic fluctuation and the variation of the hole concentration on the properties of high-T_c superconductors. In case of high-T_c superconductors, thermodynamic fluctuations are known to be of immense importance. The effect of the fluctuations can be taken into account by considering higher-order terms in the free energy functional as suggested by Ginzburg [38] for a single-order parameter (s-wave) GL theory. This can be generalized to the anisotropic two-order parameter case considered in this paper. Also an interesting problem would be to study the high-T_c cuprates by taking into account the orthorhombic distortion of the system. The presence of orthorhombic distortion gives rise to anisotropic effects even in the isotropic systems. So it would be of interest to understand the effect that will arise in the system in the presence of both orthorhombic distortions and the anisotropy introduced by the effective mass approximation. The orthorhombic distortion of the system can be taken into account by introducing suitable second-order coupling terms (i.e. $\psi_d^*\psi_s + \psi_s^*\psi_d$) in the free energy functional [39]. The method discussed in the present work can prove to be useful for the study of other multicomponent materials. The work can also be generalized to study thin films, which will give a more realistic picture of practical high-T_c superconducting materials.

References

[1] Karmakar M and Dey B 2008 *J. Phys.: Condens. Matter* **20** 255218
[2] Wollman D A, Van Harlingen D J, Giapintzakis J and Ginsberg D M 1995 *Phys. Rev. Lett.* **74** 797
[3] Iguchi I and Wen Z 1994 *Phys. Rev.* B **49** 12388
[4] Tsuei C C, Kirtley J R, Chi C C, Lock See Y-J, Gupta A, Shaw T, Sun J Z and Ketchen M B 1994 *Phys. Rev. Lett.* **73** 593
[5] Mathai A, Gim Y, Black R C, Amar A and Wellstood F C 1995 *Phys. Rev. Lett.* **74** 4523
[6] Smilde H J H, Golubov A A, Ariando, Rijnders G, Dekkers J M, Harkema S, Blank D H A, Rogalla H and Hilgenkamp H 2005 *Phys. Rev. Lett.* **95** 257001
[7] Khasanov R, Strassle S, Di Castro D, Masui T, Miyasaka S, Tajima S, Bussmann-Holder A and Keller H 2007 *Phys. Rev. Lett.* **99** 237601
[8] Khasanov R, Shengelaya A, Maisuradze A, Mattina F La, Bussmann-Holder A, Keller H and Muller K A 2007 *Phys. Rev. Lett.* **98** 057007 and references therein
[9] Hazen R M 1991 *Physical Properties of High Temperature Superconductors II* ed D M Ginsberg (Singapore: World Scientific)
[10] Sigrist M and Rice T M 1987 *Z. Phys.* B **68** 9
[11] Joynt R 1990 *Phys. Rev.* B **41** 4271
[12] Chakravarty S, Laughlin R B, Morr D K and Nayak C 2001 *Phys. Rev.* B **63** 094503
[13] Beal-Monod M T and Maki K 1996 *Europhys. Lett.* **33** 309
[14] Curras S R, Ferro G, Gonzalez M T, Ramallo M V, Ruibal M, Veira J A, Wagner P and Vidal F 2003 *Phys. Rev.* B **68** 094501
Ramallo M V, Pomar A and Vidal F 1996 *Phys. Rev.* B **54** 4341
[15] Volovik G E and Gor'kov L P 1985 *Zh. Eksp. Teor. Fiz.* **88** 1412
Volovik G E and Gor'kov L P 1985 *Sov. Phys.—JETP* **61** 843 (Engl. Transl.)
[16] Sigrist M, Rice T M and Ueda K 1989 *Phys. Rev. Lett.* **63** 1727
Bailey D B, Sigrist M and Laughlin R B 1997 *Phys. Rev.* B **55** 15239
[17] Sigrist M, Kuboki K, Lee P A, Millis A J and Rice T M 1996 *Phys. Rev.* B **53** 2835
[18] Lu D H, Feng D L, Armitage N P, Shen K M, Damascelli A, Kim C, Ronning F, Shen Z X, Bonn D A, Liang R, Hardy W N, Rykov A I and Tajima S 2001 *Phys. Rev. Lett.* **86** 4370
[19] Feng D L *et al* 2000 *Science* **289** 277
[20] Heyen E T, Cardona M, Karpinski J, Kaldis E and Rusiecki S 1991 *Phys. Rev.* B **43** 12958
[21] Limonov M F, Rykov A I, Tajima S and Yamanaka A 1998 *Phys. Rev. Lett.* **80** 825
[22] Limonov M F, Rykov A I, Tajima S and Yamanaka A 2000 *Phys. Rev.* B **61** 12412
[23] Zhang K, Bonn D A, Kamal S, Liang R, Baar D J, Hardy W N, Basov D and Timusk T 1994 *Phys. Rev. Lett.* **73** 2484
[24] Keimer B, Shih W Y, Erwin R W, Lynn J W, Dogan F and Aksay I A 1994 *Phys. Rev. Lett.* **73** 3459
[25] Maggio-Aprile I, Renner Ch, Erb A, Walker E and Fisher Ø 1995 *Phys. Rev. Lett.* **75** 2754
[26] Gohng J and Finnemore D K 1992 *Phys. Rev.* B **46** 398
[27] Xu J-H, Ren Y and Ting C S 1996 *Int. J. Mod. Phys.* **22** 2699 and references therein
[28] Franz M, Kallin C, Soininen P I, Berlinsky A J and Fetter A L 1996 *Phys. Rev.* B **53** 5795
[29] Heeb R, van Otterlo A, Sigrist M and Blatter G 1996 *Phys. Rev.* B **54** 9385
[30] Brandt E H 1997 *Phys. Rev. Lett.* **78** 2208
[31] Feder D L and Kallin C 1997 *Phys. Rev.* B **55** 559
[32] Shan L, Huang Y, Ren C and Wen H H 2006 *Phys. Rev.* B **73** 134508
[33] Sonier J E, Brewer J H and Kiefl R F 2000 *Rev. Mod. Phys.* **72** 769
[34] Hardy W N, Bonn D A, Morgan D C, Liang R and Zhang K 1993 *Phys. Rev. Lett.* **70** 3999
[35] Van der Beek C J, Konczykowski M, Abaloshev A, Abalosheva I, Gierlowski P, Lewandowski S J, Indenbom M V and Barbanera S 2002 *Phys. Rev.* B **66** 024523
[36] Karmakar M and Dey B 2006 *Phys. Rev.* B **74** 172508
[37] Achelere A and Dey B 2005 *Phys. Rev.* B **71** 224504
[38] Ginzburg V L 1988 *Physica* C **153–155** 1617
[39] Han Q and Zhang L 1997 *Phys. Rev.* B **56** 11942